Journal of Nuclear Medicine, published on March 26, 2015 as doi:10.2967/jnumed.114.150680

Title:

The Effect of Bi-terminal PEGylation of an Integrin $\alpha_v\beta_6$-Targeted ^{18}F-Peptide on Pharmacokinetics and Tumor Uptake

Running foot line:

Bi-terminally PEGylated Peptide for $\alpha_v\beta_6$

Authors:

Sven H. Hausner[1,2], Nadine Bauer[2], Lina Y. Hu[2], Leah M. Knight[1], and Julie L. Sutcliffe[1,2,3,4]

Affiliations:

1 Department of Internal Medicine, Division of Hematology/Oncology,

2 Department of Biomedical Engineering,

3 Center for Molecular and Genomic Imaging,

4 Radiochemistry Research and Training Facility,

University of California Davis, Davis and Sacramento, CA, USA.

Corresponding author:

Julie Sutcliffe. Department of Internal Medicine, 2941 Stockton Blvd, UC Davis, Sacramento, CA 95817. Tel.: 916-734-5536; fax: 916-734-7572; e-mail: jlsutcliffe@ucdavis.edu

First author:

Sven Hausner. Department of Internal Medicine, 2941 Stockton Blvd, UC Davis, Sacramento, CA 95817. Tel.: 916-734-5482; fax: 916-734-7572; e-mail: shhausner@ucdavis.edu

Word count:

4967

Financial support:

Department of Energy, Office of Science, award # DE-SC0002061;

UC Davis Research Investment in Science and Engineering grant

Abstract

Radiotracers based on the peptide A20FMDV2 selectively target the cell surface receptor integrin $\alpha_v\beta_6$. This integrin has been identified as a prognostic indicator correlating with the severity of disease for several challenging malignancies. In previous studies of A20FMDV2-peptides labeled with 4-^{18}F-fluorobenzoic acid (^{18}F-FBA), we have shown that introduction of poly(ethylene glycol) (PEG) improves pharmacokinetics, including increased uptake in $\alpha_v\beta_6$-expressing tumors. The present study evaluated the effect of site-specific *C*-terminal or dual (*N*- and *C*-terminal) PEGylation, yielding ^{18}F-FBA-A20FMDV2-PEG$_{28}$ (**4**) and ^{18}F-FBA-PEG$_{28}$-A20FMDV2-PEG$_{28}$ (**5**), on $\alpha_v\beta_6$-targeted tumor-uptake and pharmacokinetics. The results are compared to ^{18}F-FBA-labeled A20FMDV2-radiotracers (**1-3**) bearing either no PEG, or different PEG units at the *N*-terminus.

Methods: The radiotracers were prepared and radiolabeled on solid phase. Using three cell lines, DX3puroβ6 [$\alpha_v\beta_6$(+)], DX3puro [$\alpha_v\beta_6$(-)], and BxPC-3 [$\alpha_v\beta_6$(+)], they were evaluated in vitro (serum stability; cell binding and internalization) and in vivo in mouse models bearing paired DX3puroβ6/DX3puro and, for **5**, BxPC-3 xenografts.

Results: Size and location of the PEG units significantly affected $\alpha_v\beta_6$-targeting and pharmacokinetics. While the *C*-terminally PEGylated **4** showed some improvements over the unPEGylated ^{18}F-FBA-A20FMDV2 (**1**), it was the bi-terminally PEGylated **5** that displayed the more favorable combination of high $\alpha_v\beta_6$-affinity, -selectivity and pharmacokinetic profile. In vitro, **5** bound to $\alpha_v\beta_6$-expressing DX3puroβ6 and BxPC-3 cells with 60.5±3.3% and 48.8±8.3%, respectively, with a significant fraction of internalization (37.2±4.0% and 37.6±4.1% of total radioactivity, respectively). By comparison, the DX3puro control showed only 3.0±0.5% binding and 0.9±0.2% internalization. In vivo, **5** maintained high, $\alpha_v\beta_6$-directed binding in the paired DX3puroβ6/DX3puro model (1 h: DX3puroβ6: 2.3±0.2% ID/g; DX3puroβ6/DX3puro ratio: 6.5/1;

4 h: 10.7/1). In the pancreatic BxPC-3 model uptake was 4.7±0.9% ID/g (1 h) despite small tumor sizes (20-80 mg).

Conclusion: The bi-PEGylated radiotracer **5** showed a greatly improved pharmacokinetic profile, beyond what was predicted from individual *N*- or *C*-terminal PEGylation. It appears that the two PEG units acted synergistically to result in an improved metabolic profile including high $\alpha_v\beta_6$(+)-tumor uptake and retention.

Key words:

Integrin $\alpha_v\beta_6$, positron emission tomography, peptide, PEGylation, metabolism

INTRODUCTION

Integrins are heterodimeric transmembrane glycoprotein receptors comprised of two noncovalently joint subunits, α and β. Only certain combinations between the known 18 α and 8 β subunits are formed, resulting in 24 integrins (*1-3*). Together, the integrin family of cell surface receptors is involved in cell binding, motility, and bidirectional signaling. Among the Arginine-Glycine-Aspartic Acid (RGD)-recognizing group, the integrin $\alpha_v\beta_3$ has received much attention due to its role in angiogenesis, wound healing, and tumor metastasis (*4-6*). More recently, the integrin $\alpha_v\beta_6$ has become the focus of intense investigations where it was found to be involved in the production of cancer promoting matrix metalloproteinases (MMPs), tumor growth factor β (TGF-β), and the facilitation of the epithelial-mesenchymal transition (EMT) (*7-9*). While expression levels are generally undetectable in healthy adult tissues, clinical studies found that $\alpha_v\beta_6$-expression is highly up-regulated in malignancies including pancreatic, basal cell, cervical, gastric, colorectal, and non-small cell lung cancer, as well as oral squamous cell carcinoma (*10-17*). Frequently, increased expression levels have been found to correlate with poor prognosis, making integrin $\alpha_v\beta_6$ an important prognostic marker.

Peptides targeting the integrin $\alpha_v\beta_6$ have been derived from one-bead-one-compound (*18*), phage-display (*17, 19-22*) and yeast-display (*23*) library screening as well as from fragments of naturally occurring protein ligands (*24-26*). From these studies, which identified peptides with seven to 20 amino acid residues, a consensus is emerging that the 7-residue RG/TDLXXL sequence (X = unspecified α-amino acid) describes a minimum motif generally advantageous for high affinity and selectivity towards $\alpha_v\beta_6$ and that additional flanking amino acids help in further improving these characteristics (*19, 27*). When the unmodified initial lead compounds were analyzed in vitro they oftentimes already possessed good binding affinities towards integrin $\alpha_v\beta_6$ (low nanomolar IC_{50}), but they performed poorly in vivo, largely because of rapid excretion,

metabolic breakdown, or trapping in non-target organs (*23, 28*). Therefore, with the goal of achieving pharmacokinetic properties required for viable molecular imaging probes, modifications such as multimerization (*29*), cyclization (*20*), grafting onto scaffolds (*23*), and attachment of biocompatible polymers (*28*) are being pursued.

The 20-amino acid peptide A20FMDV2 (sequence NAVPNLRGDLQVLAQKVART), derived from an envelope protein of the foot-and-mouth disease virus (FMDV), has been a focus of our studies (*24-26*). When the *N*-terminally 4-^{18}F-fluorobenzoyl (^{18}F-FBA) radiolabeled ^{18}F-FBA-A20FMDV2 (**1**; Fig. 1) was evaluated in mice, an uptake of 0.66±0.09% ID/g and 0.69±0.19% ID/g at 1 h was found in $\alpha_v\beta_6$-expressing DX3puroβ6 melanoma and BxPC-3 pancreatic adenocarcinoma cell xenograft tumors, respectively, while 0.21±0.07% ID/g were observed for the $\alpha_v\beta_6$-negative DX3puro control (*26, 28*). This first-generation radiotracer showed rapid washout from the $\alpha_v\beta_6$-expressing tumors and was degraded into three urine metabolites. We subsequently found that short, monodisperse poly(ethylene glycol) (PEG) units at the *N*-terminus improved uptake to 1.9±0.4% ID/g and 1.6±0.3% ID/g, respectively, for monoPEGylated ^{18}F-FBA-PEG$_{28}$-A20FMDV2 (**2**) and diPEGylated ^{18}F-FBA-(PEG$_{28}$)$_2$-A20FMDV2 (**3**) in BxPC-3 tumors at 1 h (*28*). Additionally, PEGylation suppressed washout from tumors and aided with stability; simultaneously, however, it also resulted in increased renal uptake, and, for the diPEGylated **3**, in renal trapping.

Here, in an effort to further investigate the effect of PEGylation on $\alpha_v\beta_6$-directed tumor targeting and improve the pharmacokinetic profile of A20FMDV2-derived radiotracers we investigated two different PEGylation patterns: *C*-terminally PEGylated ^{18}F-FBA-A20FMDV2-PEG$_{28}$ (**4**) and bi-terminally PEGylated ^{18}F-FBA-PEG$_{28}$-A20FMDV2-PEG$_{28}$ (**5**). The compounds were evaluated in vitro (serum stability, cell binding and internalization) and in vivo (DX3puroβ6/DX3puro and BxPC-3 mouse models) and compared to the previously studied radiotracers.

MATERIALS AND METHODS

Chemistry and Radiochemistry

Peptide synthesis and radiolabeling were done on solid phase (*30*) and the radiotracer was formulated in phosphate buffered saline (PBS) using reagents described in the Supplemental Information.

In Vitro Studies

Radiotracer affinity to and internalization into DX3puroβ6, DX3puro, and BxPC-3 cells was determined as previously described (*30, 31*). To evaluate serum-stability, mouse serum (0.5 mL) was combined with the radiotracer (12.5 μL; 0.74 MBq) and kept at 37ºC (*31, 32*). Following precipitation of serum proteins (ethanol) the percentage of intact radiotracer was determined by HPLC.

Animal Studies

Female athymic nude mice (Charles River Laboratories; Wilmington, MA) were handled following procedures approved by the University of California, Davis, Animal Use and Care Committee, and inoculated subcutaneously either with 3×10^6 DX3puro and 3×10^6 DX3puroβ6 cells on opposite flanks, or with 3.5×10^6 BxPC-3 cells. Imaging was conducted once tumors had reached a maximum diameter of ~0.3-0.6 cm. The radiotracer (imaging: 6.5-9.0 MBq/animal; biodistribution: 1.1-2.0 MBq/animal) was injected intravenously into the tail vein of mice anesthetized with 2% isoflurane in oxygen.

For imaging studies, two animals/scan were placed side-by-side in a feet-first, prone position (*n*=4 total/tumor model/radiotracer; anesthesia: 1.5-2.0% isoflurane). PET/CT scans (dynamic 4×15-min PET emission scan starting 15 min p.i., single-frame 15-min PET emission scans at 2, and 4 h p.i.) were acquired as previously described (*31*).

For biodistribution studies, the mice were anesthetized (4% isoflurane), sacrificed and dissected (n=3/time point/tumor model/radiotracer; 1, 2, and 4 h p.i.). For blocking experiments, ^{19}F-FBA-PEG$_{28}$-A20FMDV2 (30 mg/kg, 10 mg/mL in saline) was injected intravenously (n=3) ten minutes before the radiotracer (*28*). Tissues were collected, rinsed, and radioactivity measured in a γ-counter (*31*). Calibrated, decay-corrected radioactivity concentrations are expressed as percent of injected dose per gram of sample (% ID/g). Urine was collected when possible; proteins were precipitated (ethanol), and supernatant-aliquots analyzed by HPLC.

Tumor Autoradiography, Immunohistochemistry, and Radiotracer Stability in Tumor

Following intravenous radiotracer injection (37 MBq/animal) tumor tissue was collected (1 h p.i.), embedded in freezing medium, and sectioned (*31*). Autoradiography samples were exposed to a storage phosphor-screen. For immunohistochemical $\alpha_v\beta_6$-staining sections were fixed in periodate-lysine-paraformaldehyde solution, treated with hydrogen peroxide/PBS, incubated with anti-integrin β_6 antibody and a peroxidase-labeled secondary antibody (anti goat-Ig), developed with 3,3'-diaminobenzidine (DAB), counterstained with Mayer's Hematoxylin, and mounted (DPX mounting medium).

To determine radiotracer stability, tumor tissue was collected 1 h p.i., homogenized, proteins precipitated (ethanol), and supernatant-aliquots analyzed by HPLC (*31*).

RESULTS

Chemistry and Radiochemistry

Non-radioactive ^{19}F-**4** and ^{19}F-**5** were obtained in >98% purity after HPLC purification; ^{19}F-**4**: MS (MALDI) m/z = 3587.5413 $[M+H]^+$, calcd M ($C_{159}H_{284}FN_{33}O_{57}$) 3587.0323; ^{19}F-**5**: MS (MALDI) m/z = 4891.2339 $[M+H]^+$, calcd M ($C_{218}H_{401}FN_{34}O_{86}$) 4890.8034. The corresponding ^{18}F-radiotracers, prepared by solid-phase radiolabeling with ^{18}F-FBA (22.4±4.1 GBq), were obtained in >95% radiochemical purity (synthesis time = 137±5 min; n = 7; Fig. S1) with specific

activities >75 GBq/μmol and decay-corrected radiochemical yields of 14.9±6.2% and 8.9±1.4%, respectively, for **4** and **5**.

In Vitro Studies

Both radiotracers, ^{18}F-FBA-A20FMDV2-PEG$_{28}$ (**4**) and ^{18}F-FBA-PEG$_{28}$-A20FMDV2-PEG$_{28}$ (**5**), were stable in PBS (≥4 h); in mouse serum 76% and 80% remained intact, respectively, after 60 min at 37ºC. Both radiotracers showed high $\alpha_v\beta_6$-targeted binding to and internalization into cells (Fig. 2): 32±5% of **4** bound to DX3puroβ6 and 25±3% to BxPC-3, while 4.5±0.5% bound to the DX3puro control; for both $\alpha_v\beta_6$-expressing cell lines 13% (of total radioactivity) was internalized. By comparison, for **5** binding to $\alpha_v\beta_6$-expressing cells was nearly twice as high (DX3puroβ6: 61±3%, BxPC-3: 49±8%) and internalization tripled to 37±4% and 38±4%, respectively; for the DX3puro control binding and internalization remained low (≤3%).

The resulting uptake ratio for the DX3puroβ6/DX3puro pair was 7.1/1 for radiotracer **4** ($P = 3 \times 10^{-5}$) and 20/1 for radiotracer **5** ($P = 9 \times 10^{-7}$), and the corresponding internalization ratios were 9.4/1 and 41/1, respectively ($P = 0.0001$, $P = 8 \times 10^{-5}$).

In Vivo Studies

The two new radiotracers, **4** and **5**, were evaluated in the paired DX3puroβ6/DX3puro tumor model (Fig. 3, 4; Table 1). ^{18}F-FBA-A20FMDV2-PEG$_{28}$ (**4**) was well retained in the $\alpha_v\beta_6$-expressing DX3puroβ6 tumor for the first two hours (1 h: 1.3±0.3% ID/g; 2 h: 1.0±0.01% ID/g), but then dropped to 0.27±0.07% ID/g at 4 h; uptake in the $\alpha_v\beta_6$-negative DX3puro tumor was 0.46±0.13% ID/g at 1 h, dropping to 0.11±0.02% ID/g at 4 h. The DX3puroβ6 tumor/DX3puro tumor ratios were >2.5/1 and DX3puroβ6 tumor/blood ratios were >2/1 throughout (both: $P \leq 0.02$; Fig. 3B). Uptake of ^{18}F-FBA-PEG$_{28}$-A20FMDV2-PEG$_{28}$ (**5**) in the DX3puroβ6 tumor was 2.3±0.2% ID/g at 1 h, before stabilizing at 1.4±0.2% ID/g (2 and 4 h); uptake in the $\alpha_v\beta_6$-negative DX3puro tumor was 0.39±0.12% ID/g at 1 h, dropping to 0.14±0.04% ID/g at 4 h. DX3puroβ6 tumor size did not affect radiotracer uptake and even tumors weighing less than 50 mg were

reliably detected (Fig. S5). DX3puroβ6 tumor/DX3puro tumor ratios were >6.0:1 and DX3puroβ6 tumor/blood ratios were >4.5/1 throughout for radiotracer **5** (both: $P \leq 0.001$; Fig. 4B).

Renal clearance was the major route of elimination for both radiotracers. ^{18}F-FBA-A20FMDV2-PEG$_{28}$ (**4**) showed modest kidney uptake of 17±2% ID/g at 1 h, dropping to 2.1±0.4% ID/g at 4 h. Kidney uptake of ^{18}F-FBA-PEG$_{28}$-A20FMDV2-PEG$_{28}$ (**5**) was higher (67±12% ID/g at 1 h) but also dropped over time (19±2% ID/g at 4 h). Other organs with elevated levels of radioactivity for both radiotracers were the gall bladder, stomach, and intestine (all <15% ID/g at 1 h, dropping over time), indicating possible partial clearing via the hepatobiliary route. Muscle uptake was 1.0-1.6% ID/g (**4**) and 0.9% ID/g (**5**), and lung uptake ~2-3% ID/g (both radiotracers, all time points).

HPLC analysis of radioactivity extracted from DX3puroβ6 tumor revealed that for **4**, half of the radioactivity eluted metabolized with a short retention time (Fig. S3), while for **5**, the HPLC showed <20% apparent breakdown (Fig. S4). HPLC of urine samples revealed three radioactive metabolites with short retention times for **4**, whereas for **5**, the HPLC showed only a minor new peak (18%) possessing a slightly longer retention time (Fig. S2).

Because of the better overall pharmacokinetic profile, ^{18}F-FBA-PEG$_{28}$-A20FMDV2-PEG$_{28}$ (**5**) was chosen for further evaluation in a pancreatic BxPC-3 mouse model (Fig. 4, Table 1). Here, a tumor uptake of 4.7±0.9% ID/g was observed at 1 h, dropping slightly to 4.1±1.4% ID/g (2 h) and 3.4±1.3% ID/g (4 h); tumor uptake could be reduced by 92% to 0.38±0.05% ID/g (1 h; $P = 0.001$) by pre-administration of $\alpha_v\beta_6$-targeted blocking peptide. Low uptake in the pancreas (0.46±0.07% ID/g at 1 h , 0.25±0.07% ID/g at 4 h) resulted in BxPC-3/pancreas ratios of ≥9/1 ($P < 0.01$); as shown in Figure 4C, BxPC-3/muscle ratios were around 4-to-5/1 ($P < 0.04$), while BxPC-3/blood and BxPC-3/liver ratios reached >20/1 at 4 h (both: $P = 0.01$). This resulted in clearly identifiable tumors by small-animal PET imaging at 1, 2, and 4 h (Fig 5A); the only other notable organs are kidneys, bladder (urine), gall bladder, and the GI-tract. HPLC of radioactivity

extracted from the tumor 1 h after injection revealed <20% apparent breakdown (Fig. S4) and autoradiography of BxPC-3 xenograft slices showed the most pronounced uptake of radioactivity in the rim of the tumors in areas shown by immunohistochemistry to express integrin $\alpha_v\beta_6$ (Fig. 5B).

DISCUSSION

Since its discovery in pancreatic cancer (*33*), increasing data from molecular biology as well as clinical studies point to the epithelial cell surface receptor integrin $\alpha_v\beta_6$ as a potentially important diagnostic and therapeutic target of many challenging cancers, including pancreatic cancer (*7-17, 34*). To that end, several $\alpha_v\beta_6$-specific peptide ligands, sharing a 7-residue RG/TDLXXL core motif (X = unspecified α-amino acid), have been identified and used in preclinical imaging studies (*17, 19-23, 26-28, 35, 36*). Among them, the 20-amino acid peptide A20FMDV2 (*24-26, 37*) has excellent affinity and selectivity for the integrin $\alpha_v\beta_6$ and provides a good platform for the development of imaging probes, particularly when radiolabeled with fluorine-18 (*26, 28, 30*). In vitro studies showed the beneficial effects of PEGylation on $\alpha_v\beta_6$-targeted cell binding and internalization (Fig. 2); specifically, adding one PEG_{28} unit at the *N*-terminus (**2**) or, as shown in the present study, one PEG_{28} unit each at the *N*-terminus and *C*-terminus (**5**) gave the best results (>45% of total radioactivity bound to $\alpha_v\beta_6$-positive cell, and >60% of bound radioactivity internalized). By comparison, adding one PEG_{28} unit at the *C*-terminus (**4**) or two at the *N*-terminus (**3**) resulted in smaller improvements (approximately half of those seen for **2** and **5**). Regardless of PEGylation pattern, binding to the $\alpha_v\beta_6$-negative control DX3puro cells remained low (<5% of total radioactivity). Because both DX3-cell lines express similar levels of other RGD-directed integrins, including $\alpha_v\beta_3$, $\alpha_v\beta_5$, $\alpha_v\beta_8$, and $\alpha_5\beta_1$ (*26*), these results confirm that the increased affinity of the PEGylated radiotracers did not diminish the high selectivity for integrin $\alpha_v\beta_6$. Still, even for promising lead compounds identified in vitro (viz **2**

and **5**), it is important to carefully evaluate their potential as imaging probes in vivo, where other, complex pharmacokinetic and metabolic factors come into play.

Beneficial in vivo-effects of PEGylation (*38*) on stability, pharmacokinetics, as well as tumor uptake and retention have previously been described for other PET radiotracers, for example the integrin $\alpha_v\beta_3$-targeting cyclo-RGD peptides (*39*). Similarly, we found significant in vivo-effects of PEGylation on tumor-targeting and pharmacokinetics: while the unmodified ^{18}F-FBA-A20FMDV2 (**1**) did show $\alpha_v\beta_6$-targeted tumor uptake, it also suffered from washout (BxPC-3 model: 0.69±0.19% ID/g at 1 h, 0.12±0.03% ID/g at 4 h (*28*)) and metabolic breakdown (Fig. S2). *N*-terminal incorporation of one or two PEG_{28} units significantly increased tumor uptake and retention (BxPC-3 model: 1.5±0.04% ID/g and 2.1±0.4% ID/g at 4 h for **2** and **3**, respectively (*28*)) and reduced the number of metabolites found in urine (Fig. 1, S2); unfortunately, it came at a cost of increased kidney uptake, and retention (when two PEG units were introduced (**3**); Table 1).

Incorporation of PEG_{28} at the *C*-terminus demonstrated the position-sensitivity of PEGylation with respect to pharmacokinetics: while ^{18}F-FBA-PEG_{28}-A20FMDV2 (**2**) had a steady tumor uptake of 0.5±0.1% ID/g (DX3puroβ6, 1 and 4 h (*28*)), ^{18}F-FBA-A20FMDV2-PEG_{28} (**4**) had higher tumor uptake early on, followed by washout (DX3puroβ6: 1.3±0.3% ID/g at 1 h to 0.27±0.07% ID/g at 4 h; Fig. 3). Both **2** and **4** showed identical renal clearance (Table 1), but while HPLC of urine indicated one main metabolite for **2**, three metabolites were found for **4** (Fig. S2). The latter pattern is similar to that seen for the unmodified ^{18}F-FBA-A20FMDV2 (**1**); together with the observed washout from tumor, these data indicate that *C*-terminal PEGylation conferred better tumor targeting but poorer protection from metabolic breakdown and washout from the $\alpha_v\beta_6$(+)-tumor.

Bi-terminal PEGylation further improved both DX3puroβ6 tumor uptake (**5**: 2.3±0.2% ID/g at 1 h) and retention (1.4±0.2% ID/g at 2 and 4 h), resulting in largely improved DX3puroβ6/tissue ratios for key tissues including muscle, liver, and the control DX3puro tumor; uptake in the latter

was the same for **4** and **5** (Fig. 3, 4, Table 1). A notable exception was the kidneys: their initial uptake increased (similar to the results obtained when adding a second PEG_{28} unit at the *N*-terminus, i.e. going from **2** to **3**), but, unlike for **3**, the radioactivity did wash out over time (Table 1). Because expression of integrin $\alpha_v\beta_6$ in murine kidneys has been shown to be negligible (*37, 40*) the renal retention of radiotracer is not target-mediated and can likely be improved by further modifications of the radiotracer. HPLC analysis of DX3puroβ6 tumor homogenates showed considerably less metabolic breakdown for **5** than for **4** (<20% *vs.* 50%); given this increased apparent stability and the promising biodistribution data, specifically the good retention in the DX3puroβ6 tumors and the DX3puroβ6/organ ratios, we were encouraged to evaluate **5** further in the BxPC-3 model, a human pancreatic carcinoma cell line that endogenously expresses the integrin $\alpha_v\beta_6$. Here, tumor uptake more than doubled compared to the DX3puroβ6 model (Table 1), resulting in favorable tumor/organ ratios, including tumor/pancreas ≥9/1 and tumor/muscle 4-to-5/1 (Fig. 4). Importantly for the detection of early lesions, all tumors did show good radiotracer uptake, regardless of size (20-80 mg) or time point (Fig. S5). This, along with the washout from healthy organs, resulted in clearly identifiable tumors in PET/CT images (Fig. 5); autoradiography and immunohistochemistry confirmed co-localization of radioactivity with areas of integrin $\alpha_v\beta_6$ expression, particularly in focal points at the rim of the tumor.

Besides A20FMDV2-derived radiotracers, a number of peptide-based PET and SPECT imaging probes for integrin $\alpha_v\beta_6$ are currently being evaluated in mouse models (*27*), among them the 36-amino acid cystine knot peptides ^{18}F-fluorobenzoate-R_o1 and ^{64}Cu-DOTA-R_o1 (*23, 35*), and versions of the phage-screening derived TP H2009.1 (*22*) such as the 21-amino acid ^{99m}Tc-HHK (*36*) and the dimerized 10-amino acid ^{64}Cu-AcD10 (*40*); see Table S1 for peptide sequences. Although comparisons across different animal models and experimental protocols need to be approached with great caution, these studies collectively offer a context for the current state of A20FMDV2-derived radiotracers and suggest avenues for further improvement of **5**: easily

synthesized and radiolabeled on solid phase, **5** showed an $\alpha_v\beta_6$(+)-tumor uptake of 2.3±0.2% ID/g (DX3puroβ6; 1 h) and 4.7±0.9% ID/g (BxPC-3, 1 h), good $\alpha_v\beta_6$(+)-tumor retention and a DX3puroβ6/DX3puro-ratio of >6/1. These results compare favorably to literature data, including 1 h-tumor uptake (% ID/g: 0.52 [^{99m}Tc-HHK, BxPC-3], 1.46 [^{64}Cu-AcD10; H2009], approx. 2 [^{18}F-fluorobenzoate-R_o1; BxPC-3], 4.13 [^{64}Cu-DOTA-R_o1; BxPC-3]) and $\alpha_v\beta_6$(+)/$\alpha_v\beta_6$(-)-tumor uptake ratios (approx. 1.8/1 [^{18}F-fluorobenzoate-R_o1; BxPC-3/HEK-293] to 3.3/1 [^{99m}Tc-HHK; BxPC-3/HEK-293). For all of these radiotracers, including **5**, kidneys are the organ with highest uptake (it is not target-mediated as the kidneys do not express integrin $\alpha_v\beta_6$ (*37, 40*)); while the radiometalated compounds tend to show higher renal uptake and retention (as seen for ^{99m}Tc-HHK and ^{64}Cu-DOTA-R_o1) significant reductions are possible through thoughtful modifications (as demonstrated for ^{64}Cu-AcD10 where the acetylation of the amine functionalities was responsible for a 75% reduction in kidney uptake to 5.4±0.9% ID/g 24 h p.i.). Similarly, modifications to the peptide can also help with renal clearance of fluorine-18 labeled peptide radiotracers for integrin $\alpha_v\beta_6$ (*28, 35*). We therefore are confident that the increased kidney uptake observed for ^{18}F-FBA-PEG_{28}-A20FMDV2-PEG_{28} (**5**) can be mitigated by further modifications such as elimination of positively charged sites, multimerization (*40*) and introduction of carefully chosen steric restrictions (*35*) without negatively affecting $\alpha_v\beta_6$-targeted tumor uptake.

CONCLUSION

The radiotracers ^{18}F-FBA-A20FMDV2-PEG_{28} (**4**) and ^{18}F-FBA-PEG_{28}-A20FMDV2-PEG_{28} (**5**) were prepared and compared to other A20FMDV2 peptide-derived radiotracers. In vitro and in vivo studies showed that both size and location of the PEG units significantly affected $\alpha_v\beta_6$-targeting and pharmacokinetics. The bi-PEGylated radiotracer ^{18}F-FBA-PEG_{28}-A20FMDV2-PEG_{28} in particular showed a greatly improved pharmacokinetic profile, beyond what was predicted from individual *N*- or *C*-terminal PEGylation, making it a lead candidate for further

optimization and translational studies. To that end, work is currently under way to elucidate the metabolic fate and further improve the biodistribution profile.

ACKNOWLEDGEMENT

We thank the staff of the CMGI at UC Davis, David Boucher, and Ryan Davis. Funding: Department of Energy, Office of Science, award # DE-SC0002061; UC Davis Research Investment in Science and Engineering grant.

REFERENCES

1. Hynes RO. Integrins: bidirectional, allosteric signaling machines. *Cell.* 2002;110:673-687.

2. Srichai MN, Zent R. Integrin structure and function. In: Zent R, Pozzi A., eds. *Cell-Extracellular Matrix Interactions in Cancer*. New York, NY: Springer; 2010:19-41.

3. Takada Y, Ye X, Simon S. The integrins. *Genome Biol.* 2007;8:215.1-215.9.

4. Wadas TJ, Wong EH, Weisman GR, Anderson CJ. Coordinating radiometals of copper, gallium, indium, yttrium, and zirconium for PET and SPECT imaging of disease. *Chem Rev.* 2010;110:2858-2902.

5. Desgrosellier JS, Cheresh DA. Integrins in cancer: biological implications and therapeutic opportunities. *Nat Rev Cancer.* 2010;10:9-22.

6. Beer AJ, Schwaiger M. Imaging of integrin alpha(v)beta(3) expression. *Cancer Metastasis Rev.* 2008;27:631-644.

7. Vogetseder A, Thies S, Ingold B, et al. alpha(v)-Integrin isoform expression in primary human tumors and brain metastases. *Int J Cancer.* 2013;133:2362-2371.

8. Lu X, Lu D, Scully M, Kakkar V. The role of integrins in cancer and the development of anti-integrin therapeutic agents for cancer therapy. *Perspect Medicin Chem.* 2008;2:57-73.

9. Bandyopadhyay A, Raghavan S. Defining the role of integrin alpha(v)beta(6) in cancer. *Curr Drug Targets.* 2009;10:645-652.

10. Li HX, Zheng JH, Fan HX, Li HP, Gao ZX, Chen D. Expression of alpha(v)beta(6) integrin and collagen fibre in oral squamous cell carcinoma: association with clinical outcomes and prognostic implications. *J Oral Pathol Med.* 2013;42:547-556.

11. Sipos B, Hahn D, Carceller A, et al. Immunohistochemical screening for beta(6)-integrin subunit expression in adenocarcinomas using a novel monoclonal antibody reveals strong up-regulation in pancreatic ductal adenocarcinomas in vivo and in vitro. *Histopathology.* 2004;45:226-236.

12. Marsh D, Dickinson S, Neill GW, Marshall JF, Hart IR, Thomas GJ. Alpha(v)beta(6) integrin promotes the invasion of morphoeic basal cell carcinoma through stromal modulation. *Cancer Res.*2008;68:3295-3303.

13. Hazelbag S, Kenter GG, Gorter A, et al. Overexpression of the alpha(v)beta(6) integrin in cervical squamous cell carcinoma is a prognostic factor for decreased survival. *J Pathol.* 2007;212:316-324.

14. Zhang ZY, Xu KS, Wang JS, et al. Integrin alpha(v)beta(6) acts as a prognostic indicator in gastric carcinoma. *Clin Oncol.* 2008;20:61-66.

15. Bates RC. Colorectal cancer progression - Integrin alpha(v)beta(6) and the epithelial-mesenchymal transition (EMT). *Cell Cycle.* 2005;4(10):1350-1352.

16. Yang SB, Du Y, Wu BY, et al. Integrin alpha(v)beta(6) promotes tumor tolerance in colorectal cancer. *Cancer Immunol Immunother.* 2012;61:335-342.

17. Elayadi AN, Samli KN, Prudkin L, et al. A peptide selected by biopanning identifies the integrin alpha(v)beta(6) as a prognostic biomarker for nonsmall cell lung cancer. *Cancer Res.* 2007;67:5889-5895.

18. Gagnon MKJ, Hausner SH, Marik J, Abbey CK, Marshall JF, Sutcliffe JL. High-throughput in vivo screening of targeted molecular imaging agents. *Proc Natl Acad Sci U S A.* 2009;106:17904-17909.

19. Kraft S, Diefenbach B, Mehta R, Jonczyk A, Luckenbach GA, Goodman SL. Definition of an unexpected ligand recognition motif for alpha(v)beta(6) integrin. *J Biol Chem.* 1999;274:1979-1985.

20. Hsiao JR, Chang Y, Chen YL, et al. Cyclic alpha(v)beta(6)-targeting peptide selected from biopanning with clinical potential for head and neck squamous cell carcinoma. *Head Neck.* 2010;32:160-172.

21. Nothelfer EM, Zitzmann-Kolbe S, Garcia-Boy R, et al. Identification and characterization of a peptide with affinity to head and neck cancer. *J Nucl Med.* 2009;50:426-434.

22. Oyama T, Sykes KF, Samli KN, Minna JD, Johnston SA, Brown KC. Isolation of lung tumor specific peptides from a random peptide library: generation of diagnostic and cell-targeting reagents. *Cancer Lett.* 2003;202:219-230.

23. Kimura RH, Teed R, Hackel BJ, et al. Pharmacokinetically stabilized cystine knot peptides that bind alpha(v)beta(6) integrin with single-digit nanomolar affinities for detection of pancreatic cancer. *Clin Cancer Res.* 2012;18:839-849.

24. Logan D, Abughazaleh R, Blakemore W, et al. Structure of a major immunogenic site on foot-and-mouth-disease virus. *Nature.* 1993;362:566-568.

25. Jackson T, Sheppard D, Denyer M, Blakemore W, King AMQ. The epithelial integrin alpha(v)beta(6) is a receptor for foot-and-mouth disease virus. *J Virol.* 2000;74:4949-4956.

26. Hausner SH, DiCara D, Marik J, Marshall JF, Sutcliffe JL. Use of a peptide derived from foot-and-mouth disease virus for the noninvasive imaging of human cancer: generation and evaluation of 4-^{18}F-fluorobenzoyl A20FMDV2 for in vivo imaging of integrin alpha(v)beta(6) expression with positron emission tomography. *Cancer Res.* 2007;67:7833-7840.

27. Liu H, Wu Y, Wang F, Liu Z. Molecular imaging of integrin alpha(v)beta(6) expression in living subjects. *Am J Nucl Med Mol Imaging.* 2014;4:333-345.

28. Hausner SH, Abbey CK, Bold RJ, et al. Targeted in vivo imaging of integrin alpha(v)beta(6) with an improved radiotracer and its relevance in a pancreatic tumor model. *Cancer Res.* 2009;69:5843-5850.

29. Gray BP, McGuire MJ, Brown KC. A liposomal drug platform overrides peptide ligand targeting to a cancer biomarker, irrespective of ligand affinity or density. *PLoS One.* 2013;8:e72938.

30. Hausner SH, Kukis DL, Gagnon MKJ, et al. Evaluation of [^{64}Cu]Cu-DOTA and [^{64}Cu]Cu-CB-TE2A chelates for targeted positron emission tomography with an alpha(v)beta(6)-specific peptide. *Mol Imaging.* 2009;8:111-121.

31. Hausner SH, Bauer N, Sutcliffe JL. In vitro and in vivo evaluation of the effects of aluminum ^{18}F-fluoride radiolabeling on an integrin alpha(v)beta(6)-specific peptide. *Nucl Med Biol.* 2014;41:43-50.

32. Gottumukkala V, Heinrich TK, Baker A, et al. Biodistribution and stability studies of ^{18}F-fluoroethylrhodamine B, a potential PET myocardial perfusion agent. *Nucl Med Biol.* 2010;37:365-370.

33. Sheppard D, Rozzo C, Starr L, Quaranta V, Erle DJ, Pytela R. Complete amino-acid-sequence of a novel integrin beta subunit (beta6) identified in epithelial-cells using the polymerase chain-reaction. *J Biol Chem.* 1990;265:11502-11507.

34. Yang G-Y, Xu K-S, Pan Z-Q, et al. Integrin alpha(v)beta(6) mediates the potential for colon cancer cells to colonize in and metastasize to the liver. *Cancer Sci.* 2008;99:879-887.

35. Hackel BJ, Kimura RH, Miao Z, et al. ^{18}F-Fluorobenzoate-labeled cystine knot peptides for PET imaging of integrin alpha(v)beta(6). *J Nucl Med.* 2013;54:1101-1105.

36. Liu Z, Liu H, Ma T, et al. Integrin alpha(v)beta(6)-targeted SPECT imaging for pancreatic cancer detection. *J Nucl Med.* 2014;55:989-994.

37. Saha A, Ellison D, Thomas GJ, et al. High-resolution in vivo imaging of breast cancer by targeting the pro-invasive integrin alpha(v)beta(6). *J Pathol.* 2010;222:52-63.

38. Harris JM, Chess RB. Effect of PEGylation on pharmaceuticals. *Nat Rev Drug Discov.* 2003;2:214-221.

39. Chen K, Conti PS. Target-specific delivery of peptide-based probes for PET imaging. *Adv Drug Deliver Rev.* 2010;62:1005-1022.

40. Singh AN, McGuire MJ, Li S, et al. Dimerization of a phage-display selected peptide for imaging of alpha(v)beta(6)-integrin: two approaches to the multivalent effect. *Theranostics.* 2014;4:745-760.

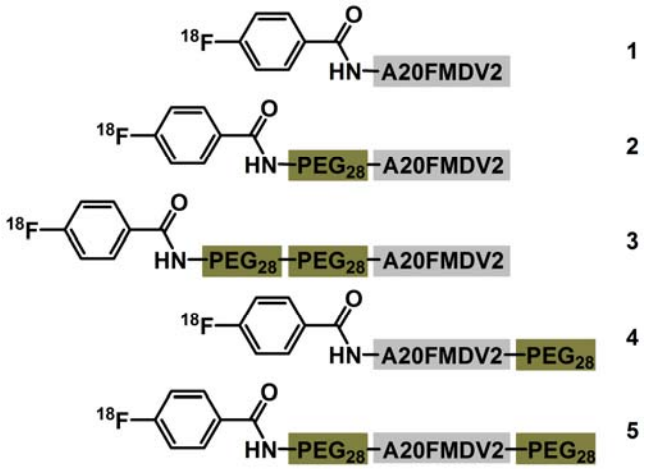

FIGURE 1: Structures of radiotracers evaluated.

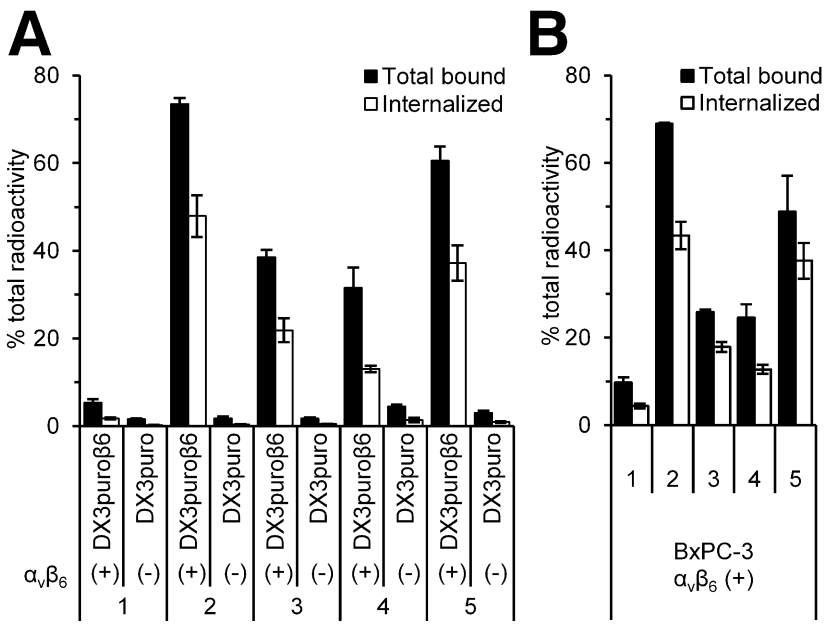

FIGURE 2: Binding and internalization of the radiotracers in vitro. (**A**) Paired, integrin $\alpha_v\beta_6$-expressing DX3puroβ6 cell line and non-$\alpha_v\beta_6$-expressing DX3puro control ($P \leq 0.0001$ for corresponding data-sets). (**B**) Integrin $\alpha_v\beta_6$-expressing BxPC-3 cell line. Filled columns: fraction of total radioactivity (n = 4/radiotracer/cell line/condition; 60 min); bars: SD. Data for **1** - **3** are from Hausner et al. (*28*).

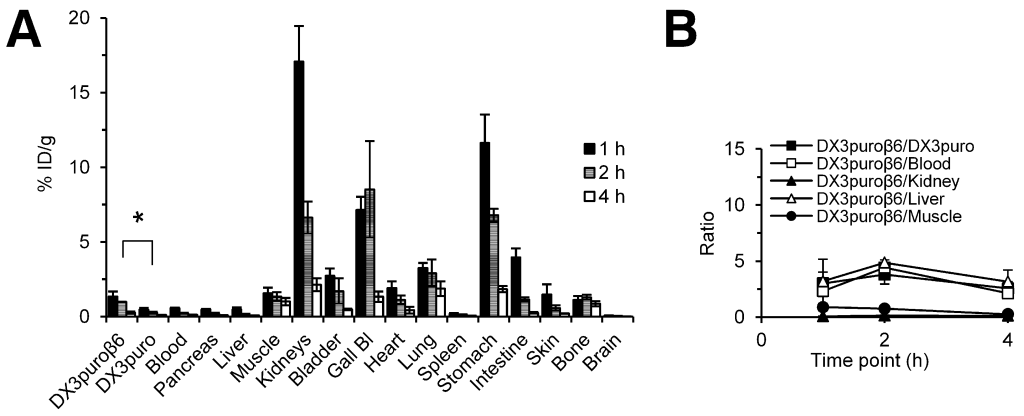

FIGRUE 3: Biodistribution data of ^{18}F-FBA-A20FMDV2-PEG$_{28}$ (**4**) in mice bearing paired $\alpha_v\beta_6$-expressing DX3puroβ6 and non-$\alpha_v\beta_6$-expressing DX3puro xenograft tumors. (**A**) Organ uptake (% ID/g; bars: SD; n = 3/time point; * $P \leq 0.02$ for corresponding time points). (**B**) Uptake ratios of **4** for tumors and selected organs (bars: SD).

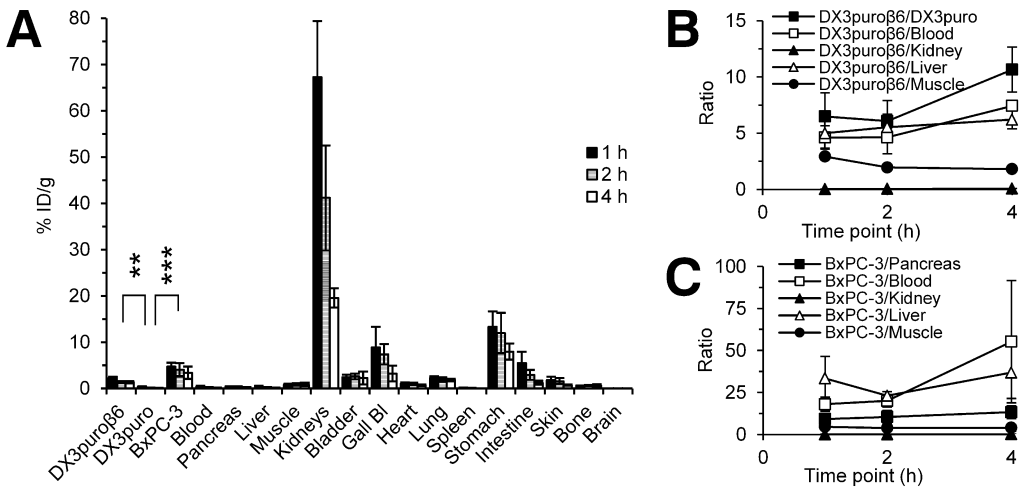

FIGURE 4: Biodistribution data of ^{18}F-FBA-PEG$_{28}$-A20FMDV2-PEG$_{28}$ (**5**) in mice bearing either paired $\alpha_v\beta_6$-expressing DX3puroβ6 and non-$\alpha_v\beta_6$-expressing DX3puro xenograft tumors, or $\alpha_v\beta_6$-expressing BxPC-3 xenograft tumors. (**A**) Organ uptake (% ID/g; bars: SD; tumors: n = 3/time point, non-tumor tissues: n = 6/time point; ** $P \leq 0.001$, *** $P \leq 0.014$ for corresponding time points). Uptake ratios of **5** for tumors and selected organs in (**B**) the paired DX3 tumor model and (**C**) the BxPC-3 tumor model (bars: SD).

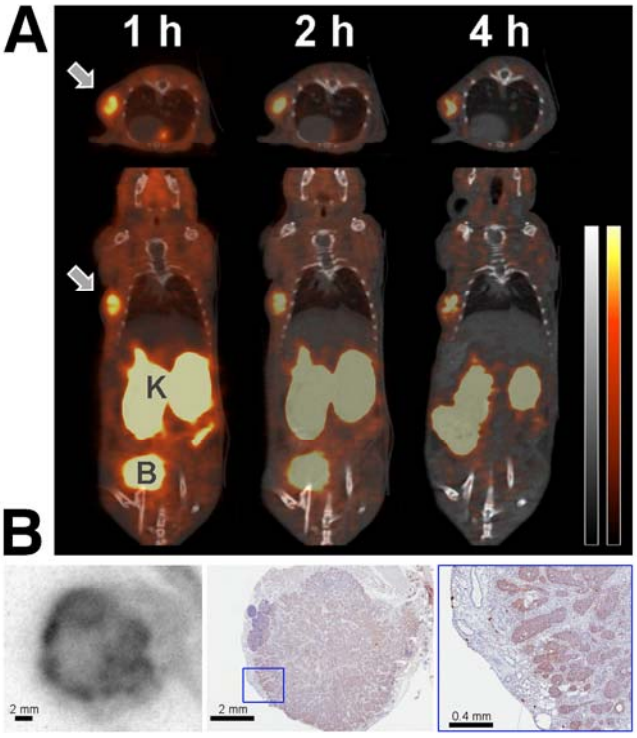

FIGURE 5: (**A**) Representative transaxial and coronal cross-sections of PET/CT images obtained after injection of ^{18}F-FBA-PEG$_{28}$-A20FMDV2-PEG$_{28}$ (**5**; 8.9 MBq) in mouse bearing BxPC-3 xenograft (66 mg; arrow). PET: red, CT: gray, K = Kidneys, B = Bladder. (**B**) Autoradiography image of BxPC-3 tumor harvested 1 h after injection of **5** (39 MBq; left) and matched adjacent immunohistochemistry slice stained for integrin $\alpha_v\beta_6$-expression (middle, right: magnified section).

TABLE 1

Radiotracer uptake in tumors and selected organs in nu/nu mouse models.

Radiotracer	Tissue*	1 h	2 h	4 h
1†	DX3puroβ6	0.66±0.09	0.28±0.03	0.06±0.00
	DX3puro	0.21±0.07	0.07±0.02	0.02±0.01
	BxPC-3	0.69±0.19	0.32±0.03	0.12±0.03
	Kidney	3.3±0.8	1.0±0.8	0.16±0.09
	Muscle	0.54±0.18	0.30±0.19	0.05±0.02
	Blood	0.21±0.07	0.07 ± 0.01	0.02±0.01
2†	DX3puroβ6	0.49±0.12	0.42±0.05	0.49±0.04
	DX3puro	0.10±0.03	0.05±0.00	0.07±0.06
	BxPC-3	1.9±0.4	1.3±0.1	1.5±0.04
	Kidney	19±5	7.4±1.8	3.3±0.7
	Muscle	0.75±0.47	0.58±0.14	0.41±0.09
	Blood	0.16±0.02	0.05±0.02	0.03±0.03
3†	DX3puroβ6	0.52±0.09	0.61±0.11	0.54±0.08
	DX3puro	0.11±0.03	0.09±0.03	0.06±0.01
	BxPC-3	1.6±0.3	2.3±0.5	2.1±0.4
	Kidney	43±13	41±7	42±5
	Muscle	0.38±0.03	0.69±0.03	0.47±0.06
	Blood	0.18±0.10	0.09±0.02	0.01±0.01
4‡	DX3puroβ6	1.3±0.3	1.0±0.01	0.27±0.07
	DX3puro	0.46±0.13	0.27±0.06	0.11±0.02
	Kidney	17±2	6.6±1.1	2.1±0.4
	Muscle	1.6±0.4	1.4±0.3	1.0±0.3
	Blood	0.57±0.03	0.23±0.02	0.12±0.02
5	DX3puroβ6	2.3±0.2	1.4±0.2	1.4±0.2
	DX3puro	0.39±0.12	0.23±0.01	0.14±0.04
	BxPC-3	4.7±0.9	4.1±1.4	3.4±1.3
	Kidney	67±12	41±11	19±2
	Muscle	0.91±0.16	0.90±0.22	0.90±0.33
	Blood	0.40±0.16	0.26±0.07	0.14±0.07

Data determined by biodistribution and expressed as % ID/g±SD (n=3/time point/compound).

* $\alpha_v\beta_6$-Positive: DX3puroβ6, BxPC-3; $\alpha_v\beta_6$-negative: DX3puro. † Data for **1 - 3** from Hausner et al. (*26, 28*). ‡ No BxPC-3 data collected (see text).